Geophys. J. Int. (1995) **121**, 459–474

Mechanisms of local earthquakes in 3-D inhomogeneous media determined by waveform inversion

J. Šílený and I. Pšenčík

Geophysical Institute, Czech Academy of Sciences, Boční II/1401, 141 31 *Praha* 4, *Czech Republic*

Accepted 1994 October 21. Received 1994 September 15; in original form 1993 August 25

SUMMARY

A method of waveform inversion for determination of a point source mechanism and its time function is developed. It allows the use of amplitudes for relocalization of the event and in a simplistic way the optimization of the structural model as well. This is accomplished by minimization of the residual norm during modelling of the data in a phase space comprising both hypocentral coordinates and structural interpolation parameters. The ray method, used to solve the forward problem, allows consideration of generally 3-D inhomogeneous isotropic media with arbitrarily curved interfaces. Seismograms generated by sources buried in such media can be inverted provided that identification of individual body-wave phases in the observed records can be made. The point source approximation restricts application of the method to weak events only. The moment tensor description advantageously allows us to investigate local seismicity, for which it is reasonable to suppose that the foci in general have a non-DC mechanism. The method includes an error analysis consisting of transformation of the data noise variance into confidence regions for volumetric, DC and CLVD parts of the retrieved moment tensor and for its principal axes (T, N and P) as well. Tests of the method were first performed on synthetic data generated for a configuration of a local seismic network near Dobrá Voda, Slovakia. In the next step, the real data from the region were inverted to obtain the mechanism of a small earthquake of local magnitude of about 2.

Key words: ray Green's functions; source mechanism; time history.

INTRODUCTION

Determination of mechanisms of weak events is of prime interest while monitoring local seismicity, because they reflect the stress pattern acting in the area under study and may help to map even its small-scale tectonic structure. Using analogue records the only applicable method is an analysis of first motions or, at most, first amplitudes picked up from the observed seismograms. These methods, which retrieve only a little information from the seismic record, often dominate the processing of digital data as well. However, digital instrumentation allows more advanced processing, aimed at earthquake source parameter retrieval, than the classical methods of first arrivals analysis. Provided that a structural model of the region under study is available, synthetic seismograms generated by various types of source can be constructed and compared with observed records in a suitable inversion scheme.

Methods for point source mechanism retrieval with simultaneous determination of the source time function for teleseismic events have been developed, e.g. by Langston (1981), Sipkin (1982), Oldenburg (1982), Nábělek (1984); some of these approaches allow determination of the source depth as well. Sophisticated source retrieval methods exist for the inversion of near-source strong motion recordings (Anderson 1991). These approaches make use of near-source data recorded by dense accelerometer arrays and provide most of the recent information about seismic sources.

There is a gap between the teleseismic and near-source approaches which is not tackled satisfactorily. For regional and local earthquakes the seismic network is usually not dense enough and the knowledge of the medium is not detailed enough to allow the reconstruction of a finite-source model as in near-source studies. In comparison with teleseismic records, seismograms of regional and local events contain much higher frequencies which make the application of teleseismic approaches dubious (Koch 1991a,b). The use of higher frequencies requires the use of more detailed models of inhomogeneous media for which

the synthetic seismograms, specifically Green's functions, should be computed.

This requirement was followed by Šílený & Panza (1992) and Šílený, Panza & Campus (1992), who used the method of modal summation to compute Green's functions in a vertically inhomogeneous medium with very fine structure. To improve their results, they used dynamic relocalization of the depth of the event, i.e. they used amplitudes to relocate the depth of the events determined from the kinematics. They also introduced a simple structural optimization, which allowed them to produce a model of the structure, which best fits the observed data.

Recently, the method was generalized for 3-D laterally varying layered isotropic structures by using ray Green's functions to solve the forward problem. The method is used in this paper to invert seismograms observed at a limited number of stations and generated by a source buried in a realistic inhomogeneous structure. The prime goal of the study is to treat local seismicity in situations in which local variations of parameters of the medium cannot be neglected. It is expected that especially weak earthquakes are sensitive to local tectonics, and therefore weak events represent our main concern. This enables us to accept a point source approximation throughout this study. The effects of the noise in the observed records on the source mechanism retrieval are also studied.

In general, observed records are convolutions of source and path effects. To resolve the former, we must be able to remove the latter, i.e. to exclude the effects of propagation from the hypocentre to the station. Since we can never be fully successful in this task, we must expect that the path effects will be projected into the mislocation of the hypocentre and spurious source complexities. To minimize these effects, we use the two following procedures.

Imperfect knowledge of the medium leads to kinematic mislocation of the hypocentre. To minimize this effect, we use dynamic relocalization. We construct Green's functions not only in the kinematically localized hypocentre but also in a grid of points around it. During the course of inversion the hypocentre is allowed to move inside this grid and its best position is selected according to the criterion of best fit of synthetic seismograms with observed records. In this case adjustments of the hypocentre coordinates represent three additional parameters to be determined during the inversion.

Since we can never have a perfect knowledge of the model, it is reasonable to allow it slight variations during the inversion. In order not to increase the number of parameters to be determined dramatically, we choose the following strategy. The Green's functions are computed for two slightly different models and the final Green's function is evaluated as a weighted sum of the two Green's functions corresponding to the different models. The criterion for the determination of the weighting factor is again the best agreement of synthetic and observed data. We may use a weighting factor common for all the stations considered or a weighting factor specified for each station separately (in this case, we are, in fact, using a different model for each source–receiver pair).

The retrieval of the source mechanism in the moment tensor description has an advantage that there is a linear relation between the data and the moment tensor components. Another advantage of this formalism is its possibility to detect deviations from shear slip, which dominates mechanisms of strong earthquakes. The mechanisms of weak events are expected to be more sensitive to the complexities of the medium and the distribution of local stresses. This is confirmed by observations of weak induced seismicity caused by human activity. Seismic events induced by mining are frequently reported to have a non-deviatoric mechanism (Wong *et al.* 1989; Wong & McGarr 1990). The volumetric components of the mechanisms of events that occurred near underground cavities were observed to be both implosive (Stickney & Sprenke, 1993) and explosive (Feignier & Young 1992). However, strong natural earthquakes were reported as well, where the foci have a non-double-couple mechanism (Kanamori *et al.* 1993).

THEORY

The inversion method being described consists of two closely related parts which we will refer to as I and II. In the first one, the linear inversion is used to invert the observed data for a specified hypocentral point and for a specified Green's function. This part provides the mechanism of the source. On the basis of the retrieved mechanism the synthetic seismograms are constructed and compared with the observed records. The L_2-norm of their difference is a measure of the 'success' of the inversion in the *a priori* specified hypocentral point and structural model. The value of this residual norm is of principal significance in the second part of the method. It is an inversion scheme, in which the hypocentral coordinates and the structural weighting factor are determined in an iterative procedure with the criterion of minimization of the residual norm of synthetics and data. It means that the linear step providing the mechanism is an 'elementary cell' of the method, which is multiply performed in the iterative scheme updating the hypocentral coordinates and structural weighting factor(s).

(I) The linear inversion yields moment tensor time functions provided that Green's functions are fixed, i.e. they are computed for a particular position of the hypocentre and structural model. The method starts with the commonly used equation relating the k-component of seismic displacement $u_k(t)$ with moment tensor time functions $M_{ij}(t)$:

$$u_k(t) = M_{ij}(t) \otimes G_{ki,j}(t), \tag{1}$$

(see, e.g., Aki & Richards 1980). Eq. (1) is written for a point source approximation in a simplified notation: $u_k(t)$ is seismic displacement at the point of observation $\mathbf{r}$ (i.e. at the location of a particular station), $M_{ij}(t)$ is a time-dependent moment tensor at the hypocentral point $\mathbf{x}$ and $G_{ki,j}(t)$ is the jth spatial derivative of Green's function $G_{ki}(\mathbf{r}, \mathbf{x}, t)$. We limit our approach to the far-field approximation, in which the Green's function operates on a time derivative of the moment tensor only. Thus eq. (1) is transformed into

$$u_k(t) = \dot{M}_{ij}(t) \otimes g_{ki,j}(t), \tag{2}$$

where g_{ki} is the far-field part of G_{ki}. From now on we call the functions $g_{ki,j}(t)$ the Green's functions. They were evaluated as complex-valued seismograms, i.e. each consisted of traveltime and complex vectorial amplitude (for

details see Červený, Molotkov & Pšenčík 1977). The linear inversion scheme retrieving the functions $\dot{M}_{ij}(t)$ was introduced by Sipkin (1982) and its modification used here is described by Šílený *et al.* (1992). The modification of Sipkin's method consists of using the triangular parametrization of the functions $\dot{M}_{ij}(t)$ suggested by Nábělek (1984), which reduces the number of parameters to be determined and thus stabilizes the inversion. When using high-frequency local seismograms, the resultant normal system of equations for weights of the parametrization triangles (possessing an advantageous block-Toeplitz symmetry) must be damped to attain numerical stability of the solution. Koch (1991a,b), on the basis of extensive synthetic tests, points out that suitable values of damping constant range in a relatively large interval which can be estimated experimentally.

The output of the linear inversion is a set of six moment tensor rate functions (MTRFs) $\dot{M}_{ij}(t)$ $(i = 1, \ldots, 3;\ j = i, \ldots, 3)$. They are generally independent, which implies a time-dependent mechanism. Since for weak events, the foci of which are of small size, we do not anticipate a change in the mechanism during the rupture process, we try to factorize the MTRFs to exclude a time variation from them. The MTRFs can be tested for linear dependence by looking for a common time function (the time derivative of the source time function) $f(t)$ and six multiplicative constants M_{ij} $(i = 1, \ldots 3;\ j = i, \ldots, 3)$ which minimize the normalized L_2-norm of the residuals

$$N_M = \left\{ \sum_{i,j=1}^{3} \int_0^T [\dot{M}_{ij}(t) - M_{ij} f(t)]^2 \, dt \right\}^{1/2} \times \left[\sum_{i,j=1}^{3} \int_0^T \dot{M}_{ij}^2(t) \, dt \right]^{-1/2}. \quad (3)$$

Here T is the duration of the whole rupture process. If the minimization of N_M with respect to $f(t)$ and M_{ij} quantities is successful, i.e. if $N_M \ll 1$, we arrive at a constant mechanism of the event described by the moment tensor M_{ij} and time dependence of the rupture given by $f(t)$, which is the time derivative of the source time function.

The problem called here factorization of the MTRFs was investigated by Ruff & Tichelaar (1990) and Vasco (1989). The former authors determine the function $f(t)$ as a weighted average of the MTRFs, which requires some *a priori* idea about the mechanism to sum individual MTRFs with correct signs. The procedure of Vasco is based on singular value decomposition of the MTRFs into 'principal components'. The part corresponding to the biggest singular value is declared to be the best source time function and the significance of the other components is checked by the F test. This approach is very effective and computationally straightforward, but it may happen that the individual principal components do not reflect real physical mechanisms in the case where they are not well separated in time.

Here we tackled the factorization of the MTRFs as a function minimization problem: the residual N_M was treated as a non-linear function of $N_t + 6$ parameters (N_t is the number of triangles used for parametrization of the MTRFs) using the Monte Carlo and simplex minimization schemes.

(II) The computation outlined in (I) is performed using Green's functions corresponding to a specific hypocentral point and to a specific model of the medium. On the basis of the output values of the MTRFs, the synthetic seismograms can be constructed and compared with observed records. We introduce the L_2-norm of their difference,

$$N_S = \left\{ \sum_{k=1}^{N} \sum_{i=1}^{3} \int_t [u_i^k(t)|^{\text{obs}} - u_i^k(t)]^2 \, dt \right\}^{1/2}, \quad (4)$$

as a measure of the success of the linear inversion. Here N is the number of three-component stations yielding the data, $u_i^k(t)^{\text{obs}}$ is the ith component of the observed seismogram recorded by the kth station, and $u_i^k(t)$ is the corresponding synthetic seismogram. To include the variation of the hypocentral point and structural model in the method we consider the Green's functions $g_{ki,j}$ to be dependent on additional parameters q_l, $l = 1, \ldots, M$, which results in dependence of the norm N_s on the q_l parameters as well:

$$N_s = N_s(q_l). \quad (5)$$

The optimization of the hypocentre localization and of the structural model consists of minimization of the norm N_s with respect to the q_l parameters.

The parameters q_l comprise the following quantities:

(i) hypocentre coordinates; $q_l = z_H$, $q_2 = x_H$, $q_3 = y_H$;

(ii) weighting factor(s) describing interpolation between two models of the medium.

There are two options:

(a) The same structural model determined by interpolation is related to all the stations. Then we introduce a parameter q_4 $(0 \le q_4 \le 1)$, where $q_4 = 0$ implies the Green's functions computed for a model, A, while $q_4 = 1$ indicates Green's functions for a model, B (the construction of Green's functions for $0 < q_4 < 1$ from $g_{ki,j}^{\mathrm{A}}$ and $g_{ki,j}^{\mathrm{B}}$ is described later). Here $M = 4$.

(b) Structural interpolation is performed for each station separately. In this case the number of weighting factors for structural interpolation is the same as the number of stations. Specifically, we have N parameters $0 \le q_{j+3} \le 1$, $j = 1, \ldots, N$. A particular parameter q_{j+3} controls evaluation of Green's functions for the jth station in a similar way to in (a): $q_{j+3} = 0$ and $q_{j+3} = 1$ imply selecting $g_{ki,l}^{\mathrm{A}}$ and $g_{ki,l}^{\mathrm{B}}$ for the jth station, respectively. In this case $M = N + 3$.

The required minimization of the norm $N_s(q_1)$ can be performed either by a linearization approach or by a point-by-point evaluation of the function (5) in a grid search for its minimum (see the Appendix).

SYNTHETIC TESTS

The method was tested on synthetic data generated for the station configuration of a local seismic network operating near a nuclear power plant in Slovakia. A 3-D inhomogeneous model of the P-wave velocity distribution is available for this region. The rather complex seismograms observed there did not allow the construction of a separate S-wave velocity distribution; it was therefore deduced from the P-wave distribution according to the relation $v_S = v_P/\sqrt{(3)}$. For the density distribution, another empirical law was used: $\rho = 1.7 + 0.2 v_P$. No attempts were made to estimate attenuation, thus the medium is considered to be perfectly elastic. The velocity model does not contain any interface. For the purpose of testing the inversion method, a

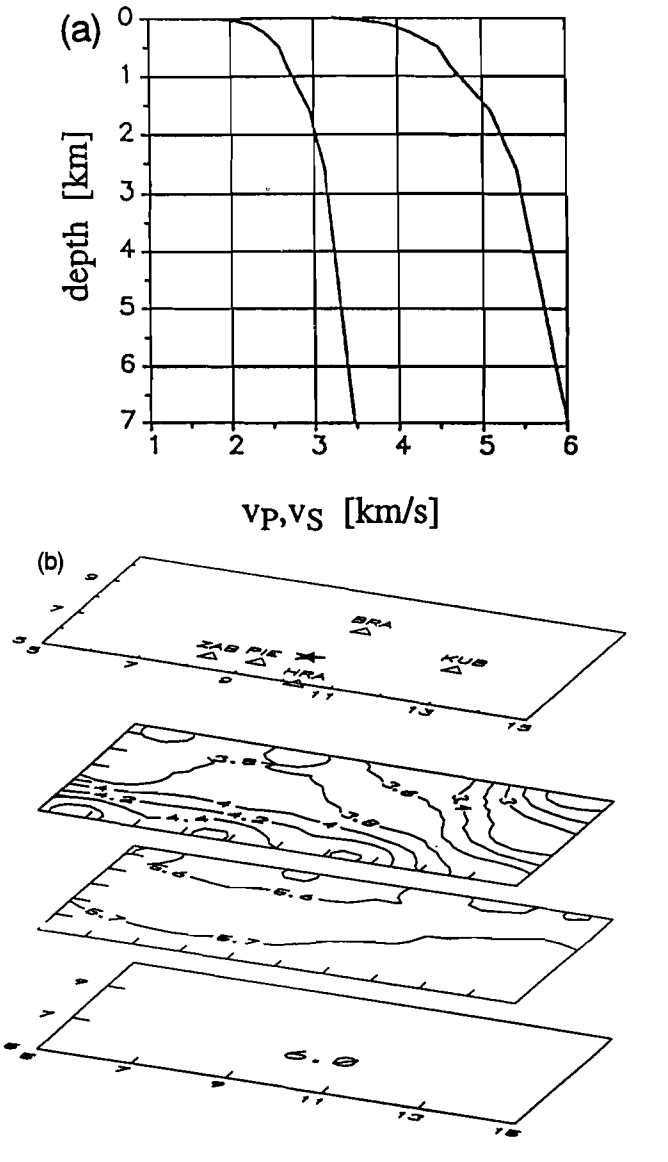

Figure 1. Structural models of the region of Dobrá Voda, Slovakia, used in synthetic tests. (a) The vertically inhomogeneous model (depth dependence of v_P and v_S shown). (b) The 3-D inhomogeneous model. Here v_P isolines are shown at depth levels 0, 3.5 and 7 km. Above the model the station distribution (triangles) and epicentre of the event (asterisk) are depicted. Coordinates are in kilometres.

vertically inhomogeneous model created by horizontal averaging of the original 3-D model was constructed and denoted as (A) (Fig. 1a). The 3-D model is marked (B) (Fig. 1b). Models A and B are very different and serve as extreme test situations. This can be seen by comparison of the projections of stations on the focal sphere. The corresponding projections in both models are mutually substantially shifted, i.e. the rays to the stations illuminate different parts of the focal sphere in different models (Fig. 2).

The synthetic tests were performed in a way simulating real processing with the objective of estimating the influence of an inexact velocity model on the source parameter determination. Ray seismograms were generated at a hypocentre in the original 3-D model with Müller pulse as source time function, and, in turn, with strike-slip and dip-slip mechanisms (see Fig. 3). The *P* arrivals were picked up and kinematic localization was performed in the

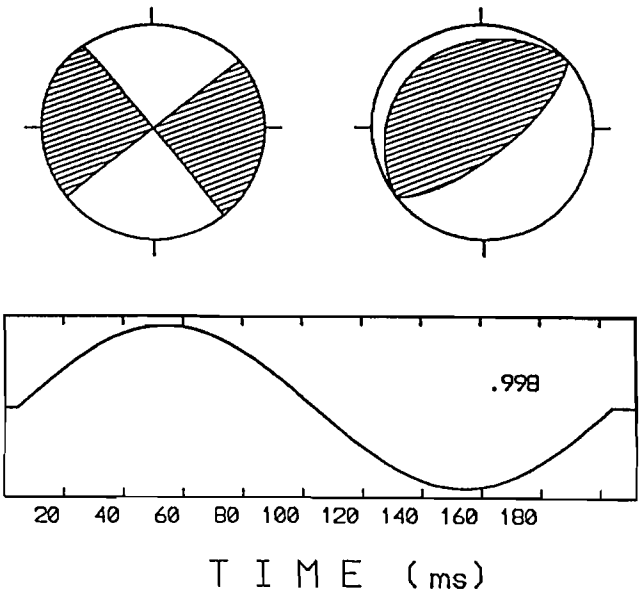

Figure 3. Parameters of the theoretical sources used for generating the synthetic data. Upper left part—mechanism of strike-slip source; upper right part—dip-slip source; lower part—source time function modelled by a Müller pulse $f(t) = \sin(n\pi t/T) - n/(n+2)\sin[(n+2)\pi t/T]$ with $T = 0.2$ s, $n = 2$. The number in the frame is the scale of the source time function.

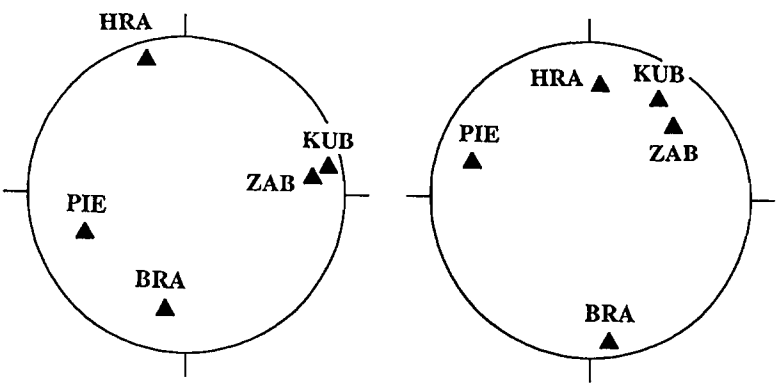

Figure 2. Equal area projections of station positions on lower focal hemisphere for the hypocentre of the test event in models A (left) and B (right).

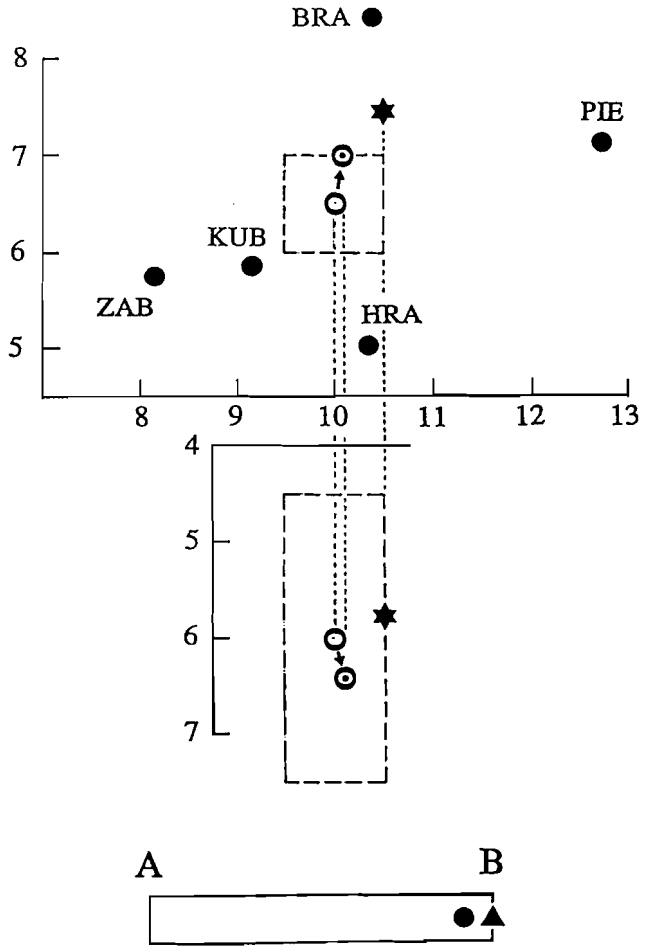

Figure 4. Dynamic relocalization of the test event (upper part) and structural optimization (bottom part). Upper part: plane view (top), front view (below); asterisk—position of the hypocentre, from which the synthetic data were generated in the 3-D inhomogeneous model; open circle—hypocentre found by kinematic localization in the vertically inhomogeneous model A; open circle with dot—the final position of the hypocentre after dynamic relocalization; full circles—stations; dashed lines—borders of the grid, around the kinematic hypocentre, in which the Green's functions are computed. Inside this box the dynamic relocalization takes place. All coordinates in kilometres. Bottom part: the result of structural optimization by using one weighting parameter for all the stations. Triangle—theoretical value of the structural weighting parameter (it indicates which model was used to generate the data); circle—resolved value of this parameter. The symbol A denotes the vertically inhomogeneous model, B the 3-D model; any point between A and B represents a transient model between A and B.

vertically inhomogeneous model A, which yielded a kinematically localized hypocentre different from that used for generation of synthetic data. Then the Green's functions were constructed in the vertices of a box situated around the localized hypocentre (see Fig. 4). The set-ups of the individual experiments together with qualitative estimates of the success of the dynamic relocalization, structure optimization and the mechanism retrieval are summarized in Table 1.

Three inversion experiments were performed with noise-free data. The first one was designed to explore the hypocentre coordinate adjustment and one structural weighting parameter optimization. During the inversion the hypocentre was relocalized properly in the horizontal direction; however, its depth localization was not improved (see Fig. 4). The resulting value of the structural parameter was obtained close to B which means the sought 3-D model (see the bottom of Fig. 4). The strike-slip mechanism was well resolved for both an unconstrained moment tensor and a deviatoric one; the source time function determined by inversion was very close to the one used for data generation, too (*cf.* Figs 3 and 5). Note that when the least-squares minimization is used, the traces with large amplitudes are modelled preferentially and are of greater significance for mechanism determination than those with small amplitudes, for which the seismograms may exhibit a poor fit. This is the case for the z-component of the BRA station, the peak amplitude of which is more than 80 times smaller than that of the x-component at the station KUB.

While inverting synthetic seismograms generated by a dip-slip source, the time function was retrieved perfectly again, but the fit of the resulting mechanism with the original one was slightly worse (*cf.* Figs 6 and 3). This is not surprising since it is a consequence of the less pronounced azimuthal dependence of amplitudes compared with the strike-slip mechanism (see Fig. 3). Note that the data correspond only to up-going rays which penetrate the upper focal hemisphere, where there are four quadrants in the sign distribution of P waves for strike-slip and only two $\pm$zones for vertical dip-slip. For inclined dip-slip in Fig. 3, there are in general only three zones covering the upper hemisphere where the P wave changes its sign.

The aim of the second test was to explore the effect of the structural optimization only, but with the option of describing it by more structural weighting parameters. Therefore, in this test the inversion was run with a fixed hypocentre and with structural weighting parameters considered for each station separately. The data were generated by a strike-slip source (Fig. 3) acting in various models of the medium for various stations: for the generation of the data for stations BRA and PIE, model A was used, while the data in stations HRA, KUB and ZAB were generated using model B (see triangles in Fig. 7a). Only P waves were included in the input data and, of course, a source was constrained to purely deviatoric moment tensor in order to find an unambiguous solution. This experiment resulted in nearly perfect resolution of the mechanisms and even better determination of the source time function (*cf.* Figs 8 and 3). As to the structure optimization, it resulted in proper structural parameter adjustment for three stations (BRA, HRA and ZAB), while for KUB and PIE the resolution was poor (see Fig. 7a). The failure in optimization of the structural parameter corresponding to station KUB may be due to low amplitudes of the data, (KUB has the lowest amplitudes of the whole data set), which are given a small weight in least-squares inversion. The reason for poor resolution of the structural interpolation parameter for station PIE must be different, because there are maximum amplitudes here from the whole data set. Because of good agreement between synthetics and data for this station, the disagreement of original and resolved values of the structural parameter for PIE indicates a small sensitivity of the quantity minimized, i.e. the $N_s(\mathbf{q})$ norm, to a change of

Table 1. Synthetic experiments for strike-slip sources.

		Test1	Test2	Test3	Test4	Test5
Objective: estimate of the influence of:		Relocalization and global structural optimization	Structural optimization (each station separately)	Structural optimization (each station separately)	Noise contamin.	Noise contamin.
data		P + S	P	P + S	P + S	P + S
number of free parameters in the iterative process (hypocentre + structure)		3 + 1	0 + 5	0 + 10	0 + 0	0 + 0
Noise		none	none	none	20 (7%)	50 (16%)
RESOLUTION	epicentre	+	fixed	fixed	fixed	fixed
	hypocentral depth	-	fixed	fixed	fixed	fixed
	structural model	++	+	+	fixed	fixed
	mechanism	++	++	++	+	-
	source time function	++	++	++	-	--

++ very well resolved, + well resolved, - poorly resolved, -- very poorly resolved

this parameter. This is caused by close values of Green's functions in both models A and B for station PIE. Note that the trace with the maximum amplitude is the z-component of PIE and that the z-component of the vector tangent at the source to the ray arriving at PIE is nearly the same in both the A and B models (see Fig. 2).

The purpose of the third experiment was to demonstrate an increase of the resolution due to extension of the data set. It was performed under the same conditions as Test 2, but the S-wave observations were also used. They were added to the previous data set as additional channels, i.e. the P and S waves recorded at the same station were considered as two independent channels, and information on the $S-P$ delay was not used. Thus, in total there were 10 structural interpolation parameters. The S waves exhibit larger amplitudes than P phases, thus they are modelled preferentially using least squares. This resulted in a good resolution of nearly all the weighting parameters corresponding to S waves (see Fig. 7b). A slightly worse (but still acceptable) fit of this parameter for PIE can be explained in the same way as in the previous test. Concerning the weighting parameters for P channels the procedure failed to determine correctly the parameter corresponding to station BRA. This is a failure of the inversion procedure because none of the three P channels was modelled well. Again it may be a consequence of the least-squares minimization applied to small amplitudes. It implies that sharply unbalanced data sets should not be inverted by the method described (here the ratio of maximum to minimum amplitudes reached a value of about 300).

With the aim of estimating the error imposed on the mechanism and source time function by the presence of noise in the seismograms, two additional experiments with synthetic data were performed. The set-up of Test 1 was chosen, but now with the **q** parameters fixed to the values obtained in the experiment referenced. The data were contaminated by random noise with frequency content close to the frequency of source time function used for data generation. Since the source time function is a Müller pulse with the period $T = 0.2$ s, the random noise was generated by using a bandpass filter between 2 and 5 Hz. The levels of its variance of 20 and 50 were *a priori* selected, which correspond roughly to 7 and 16 per cent of the peak data amplitude, respectively.

Sipkin's method (Sipkin 1982)—the linear inversion performing computation of the MTRFs (see 'Theory')—was complemented by evaluation of a covariance matrix of moment tensor functions on the basis of the variance of noise in the data. A scheme presented by Tarantola (1987) was applied; it is worth pointing out that the normal equations matrix has to be inverted, but because of its block-Toeplitz symmetry the same recursive algorithm can

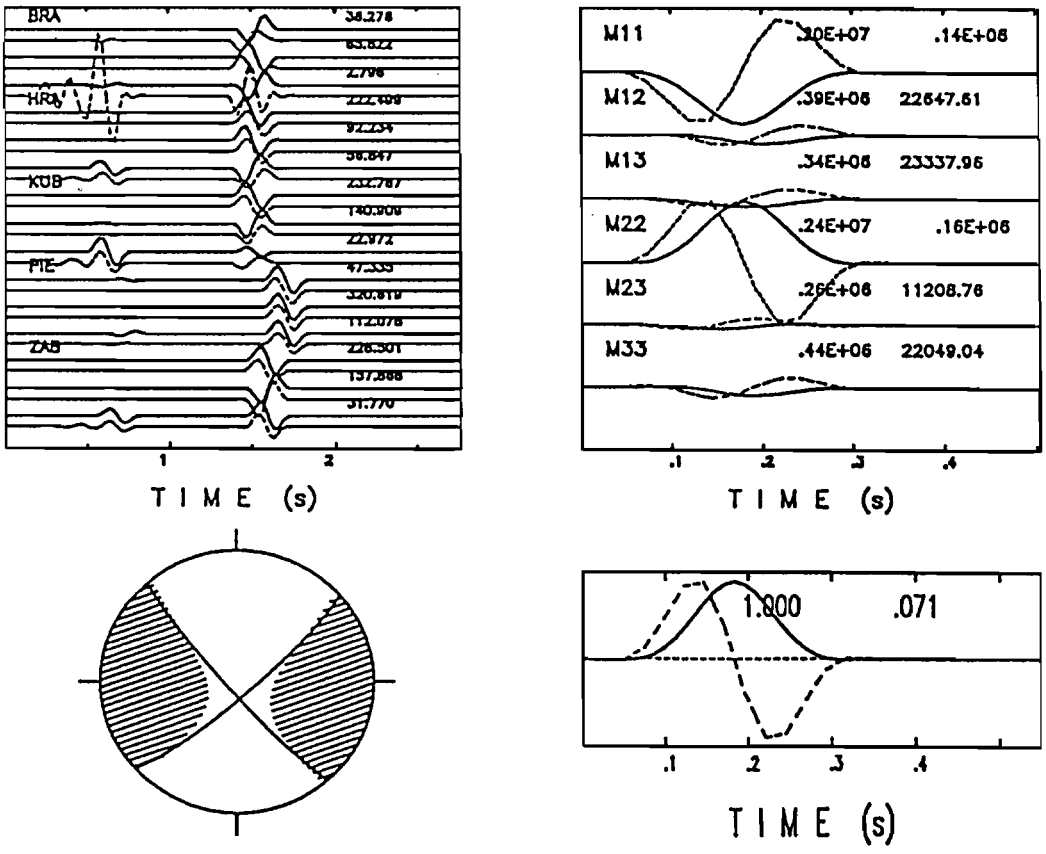

Figure 5. Source parameters retrieved by inversion of seismograms generated by strike-slip source (see Fig. 3). Upper left part—the 'data' (solid lines) and final synthetics (dashed lines); upper right part—final moment tensor rate functions $\dot{M}_{ij}(t)$ (dashed lines) together with their integrals (solid lines). Lower right part—source time function $f(t)$ (dashed line) determined by factorization of $\dot{M}_{ij}(t)$ into $M_{ij}f(t)$, and its integral (solid line); lower left part—source mechanism yielded by the moment tensor M_{ij}. Equal area projection of lower focal hemisphere. Hatched area—compressions of P waves generated by the moment source; solid lines—nodal lines of the DC component.

be used as for the determination of the moment tensor functions themselves. Then the variances of the MTRFs (with the sampling determined by their triangular parametrization) are transformed through the factorization step into a covariance matrix of the moment tensor M_{ij} and variances of source time function $f(t)$ values. These quantities are determined with respect to an *a priori* chosen probability level specifying probability content of the confidence regions to be found (the 95 per cent level was selected here). The error analysis follows an application of the first-order perturbation theory outlined by Riedesel & Jordan (1989) and results in constructing the confidence ellipses for principal axes of the M_{ij} tensor and for a vector specifying the mechanism in the Riedesel–Jordan method. (They suggested a convenient way to display the seismic moment tensor by defining a vector $\mathbf{L} = \sum \lambda_i \mathbf{e}_i$, where λ_i are eigenvalues and $\mathbf{e}_i$ are eigenvectors of the tensor M_{ij}. Its distance from the vectors $\mathbf{d} = (\mathbf{e}_1 - \mathbf{e}_3)/\sqrt{(2)}$, $\mathbf{i} = (\mathbf{e}_1 + \mathbf{e}_2 + \mathbf{e}_3)/\sqrt{(3)}$, $\mathbf{l} = (\mathbf{e}_1 - \mathbf{e}_2/2 - \mathbf{e}_3/2)/\sqrt{(3/2)}$ and $\mathbf{l}' = (\mathbf{e}_1/2 + \mathbf{e}_2/2 - \mathbf{e}_3)/\sqrt{(3/2)}$ specifies the content of a double-couple, volumetric component and CLVDs, respectively, in the mechanism.)

Results of inversion of the synthetic records contaminated by a noise of the variance $\sigma = 20$ (Test 4) are summarized in Fig. 9. The noise level was approximately comparable with amplitudes for the channels with the weakest signal (z-component of BRA, KUB and ZAB stations), reaching approximately 1/15th of the peak amplitude in the whole data set (y-component of PIE). Despite quite a high noise level severely affecting six channels of the input data set (see upper left part of Fig. 9), the mechanism of the theoretical strike-slip source was resolved well: it resulted in a pure deviatoric source, where besides a predominant DC component (78 per cent) there is a small CLVD component. However, the 95 per cent confidence ellipse of the solution vector $\mathbf{L}$ contains the vector $\mathbf{d}$, which means that the mechanism retrieved may be in this probability level a double-couple as well. Information on errors in the determination of its orientation is contained in confidence ellipses constructed for the tensional, null and pressure (T, N and P) axes, which appeared to be small in this test. The source time function (see bottom part of Fig. 9) resembles roughly the shape of a sine pulse but lacks its symmetry. Large error bars at individual time instants (depicted by lower and upper dashed lines) indicate a low precision of source time function determination.

In Test 5 the signals contaminated by the noise with $\sigma = 50$ (i.e. about 16 per cent of the peak data amplitude) were inverted. Here the noise completely destroyed eight channels by overriding the source signal, but the solution still contained information about the focus. The source mechanism consisted of a large (51 per cent) volumetric

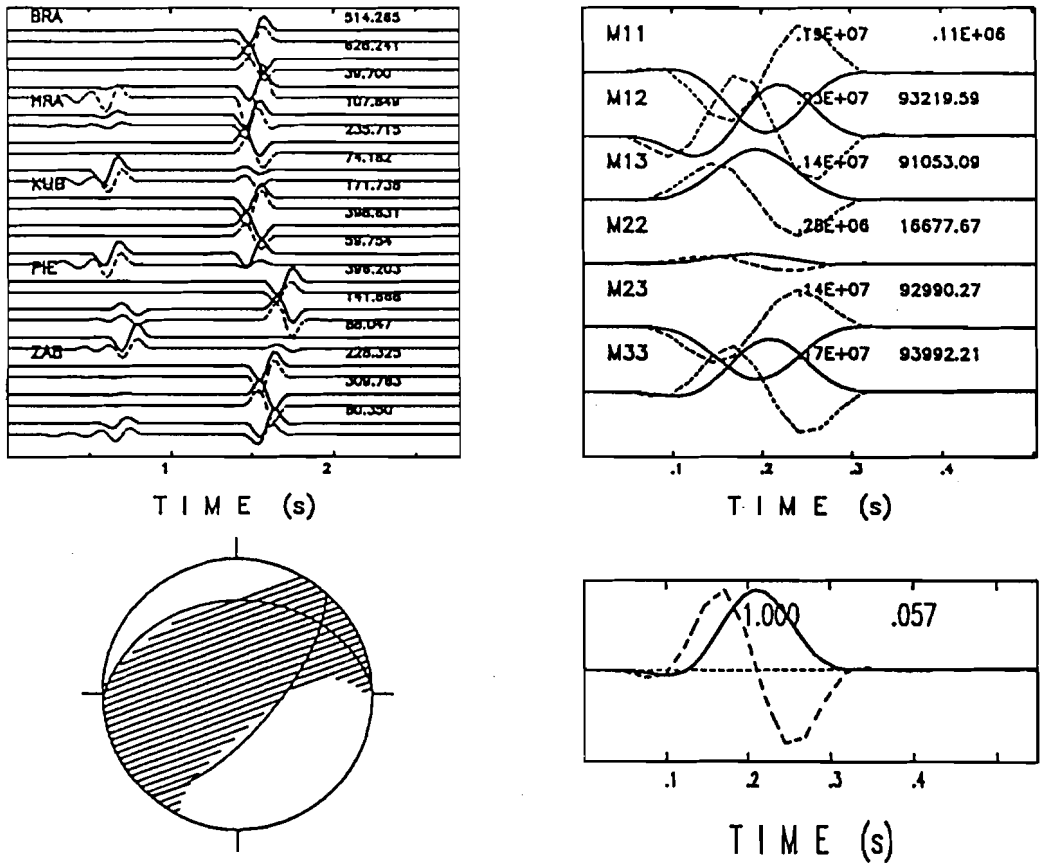

Figure 6. Source parameters retrieved by inversion of data generated by a dip-slip source (see Fig. 3). For further details see the caption of Fig. 5.

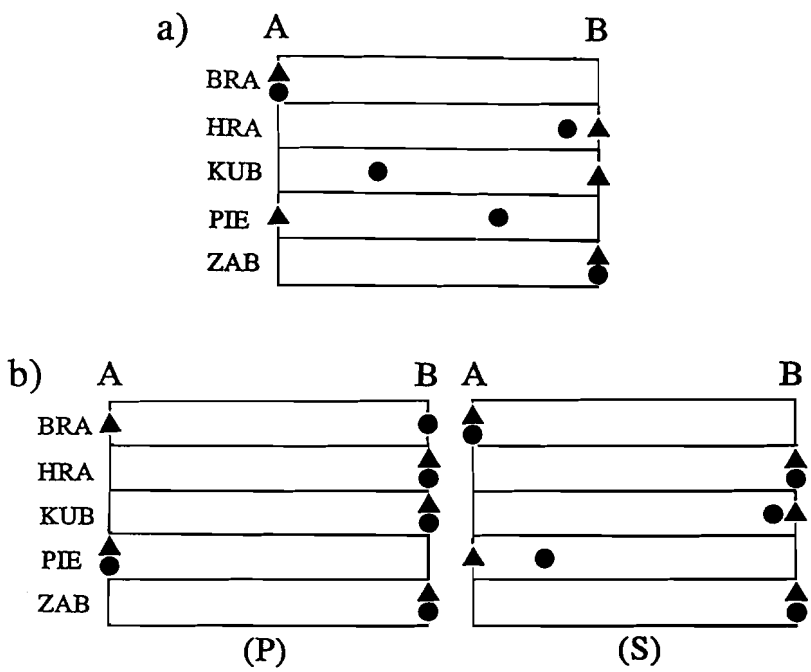

Figure 7. Results of structural optimization performed separately for each source-to-station path. Triangles—theoretical values of structural weighting parameters corresponding to individual stations; circles—resolved values of structural parameters. (a) Only *P* phases used as input data; (b) both *P* and *S* phases used as the data.

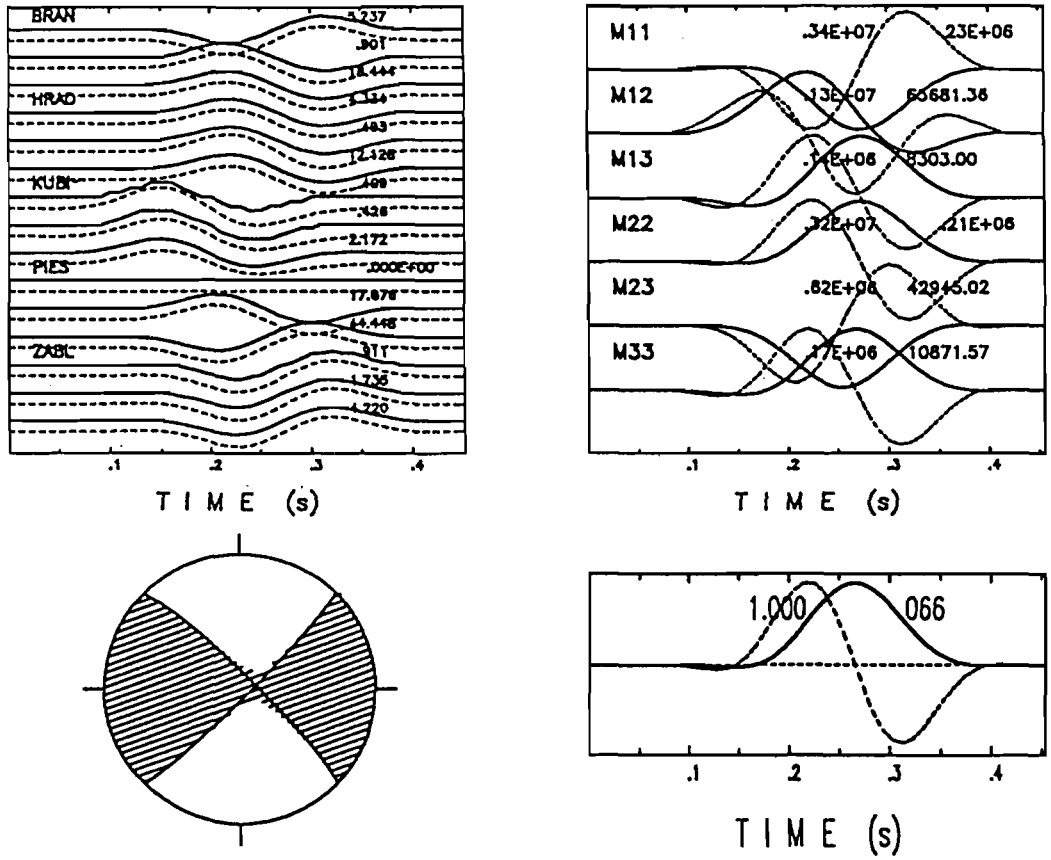

Figure 8. Source parameters determined by inversion of *P* waveforms generated by strike-slip source (see Fig. 3). Separate structural optimization for each source-to-station pair. For explanation see the caption of Fig. 5.

component of an explosive equivalent; however, its confidence at the 95 per cent probability level was very low. The appearance of a spurious volumetric source component as a result of the presence of noise in the records has already been reported by Šílený *et al.* (1992): noise has no directivity and, therefore, if attributed to the source, it is projected onto the isotropic, i.e. volumetric, component of the mechanism. The deviatoric part of the solution comprised 34 per cent DC and 66 per cent CLVD. The DC part yielded a strike-slip mechanism very close to the theoretical one, but not highly significant at the 95 per cent confidence level. The source time function was resolved very poorly which suggests that its determination is affected by noise contamination much more than the mechanism retrieval.

LOCAL EARTHQUAKE FROM THE DOBRÁ VODA REGION, SLOVAKIA

The procedure was applied to the determination of the source mechanism of a weak earthquake of magnitude about 2, recorded by the local seismic network operating near a nuclear power plant in Slovakia. This network is situated in the same region, but over a more extended area, as the one used for the synthetic tests described above (PIE is the only station common to both networks). A 3-D inhomogeneous model with sharp but continuous velocity changes is available for the region (Fig. 10a). Another model was derived from it by smoothing the inhomogeneities, and used in the inversion as an alternative to the original model (Fig. 10b). The true structure in this region is undoubtedly much more complex, which is indicated by the extreme complexity of the recorded seismograms (see velocity records in Fig. 11). They are not substantially simplified even after integration and filtration by a 10 Hz low-pass. Polarization analysis revealed very early arrivals of reflected phases after the direct *P*-wave onset, which suggests the existence of a complex near-surface system of reflectors. Such complexity is not contained in the model, thus only direct *P* phases could be inverted. From polarization analysis short portions of direct *P* waves were successfully picked up from the very beginning of the records at five of the six stations only.

Four inversion experiments were performed:

(1) fixed hypocentre and one common structural weighting parameter;

(2) fixed hypocentre and structural parameters for each station separately,

(3) variable hypocentre and a common structural parameter; and

(4) variable hypocentre and five structural parameters.

Inversions (1) and (3) (see upper part of Fig. 12) resulted in very close values of the structural parameters near 0.5, indicating that Green's functions somewhere between those for model A and those for model B were found to be the most appropriate. Comparing inversions (2) and (4) (see

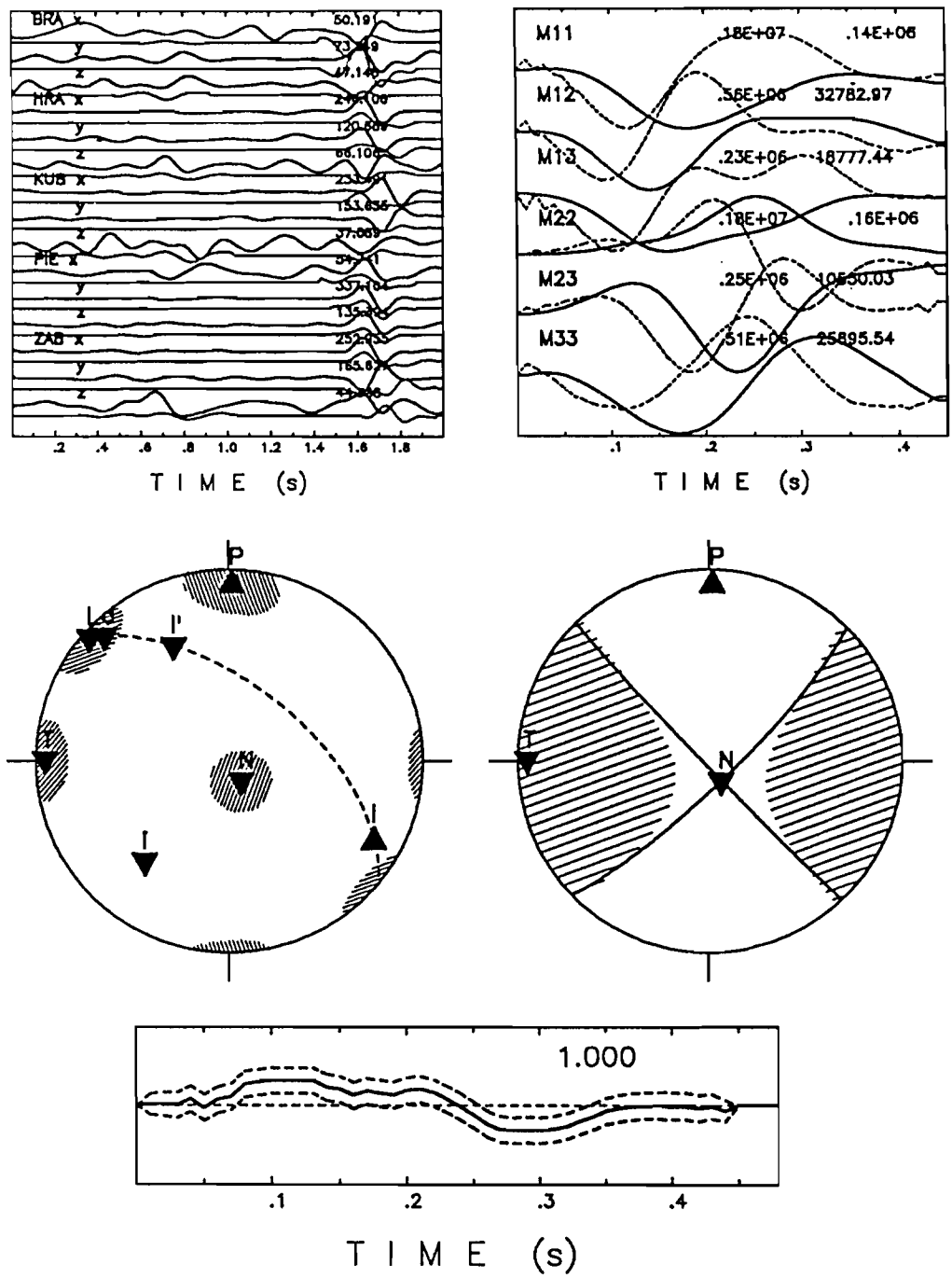

Figure 9. Inversion of records generated by a strike-slip source (Fig. 3) contaminated by random noise of variance $\sigma = 20$. Upper left part: the 'data' (thick lines) and final synthetics (thin lines). Upper right part: final moment tensor rate functions $\dot{M}_{ij}(t)$ (dashed lines) together with their integrals (solid lines). Middle right part—source mechanism yielded by the moment tensor M_{ij} (M_{ij} obtained by factorization of $\dot{M}_{ij}(t)$ into $M_{ij}f(t)$). Hatched area—compressions of P waves generated by the moment tensor source; solid lines—nodal lines of the DC component; T, N and P—principal axes of the tensor M_{ij}. Equal area projection of lower focal hemisphere. Triangle pointing downward—the vector being described intersects the lower hemisphere; triangle pointing upward—the vector intersects the upper hemisphere, but it is reversed through the centre and its intersection with the lower hemisphere is plotted. Middle left part: source mechanism plot in the Riedesel & Jordan display. **L**—the vector characterizing the mechanism; **d**, **l**, **l'** and **i**—the vectors representing a pure double-couple, two different pure compensated linear-vector dipoles, and a pure volumetric source, respectively. T, N and P—principal axes of M_{ij}. Hatched zones around **L**, T, N and P—95% confidence ellipses for the vector **L** and the principal axes of the tensor M_{ij}, respectively. Dashed line—locus of all deviatoric mechanisms. Lower part: source time function $f(t)$ (solid line) together with 95% confidence limit error bars (dashed lines).

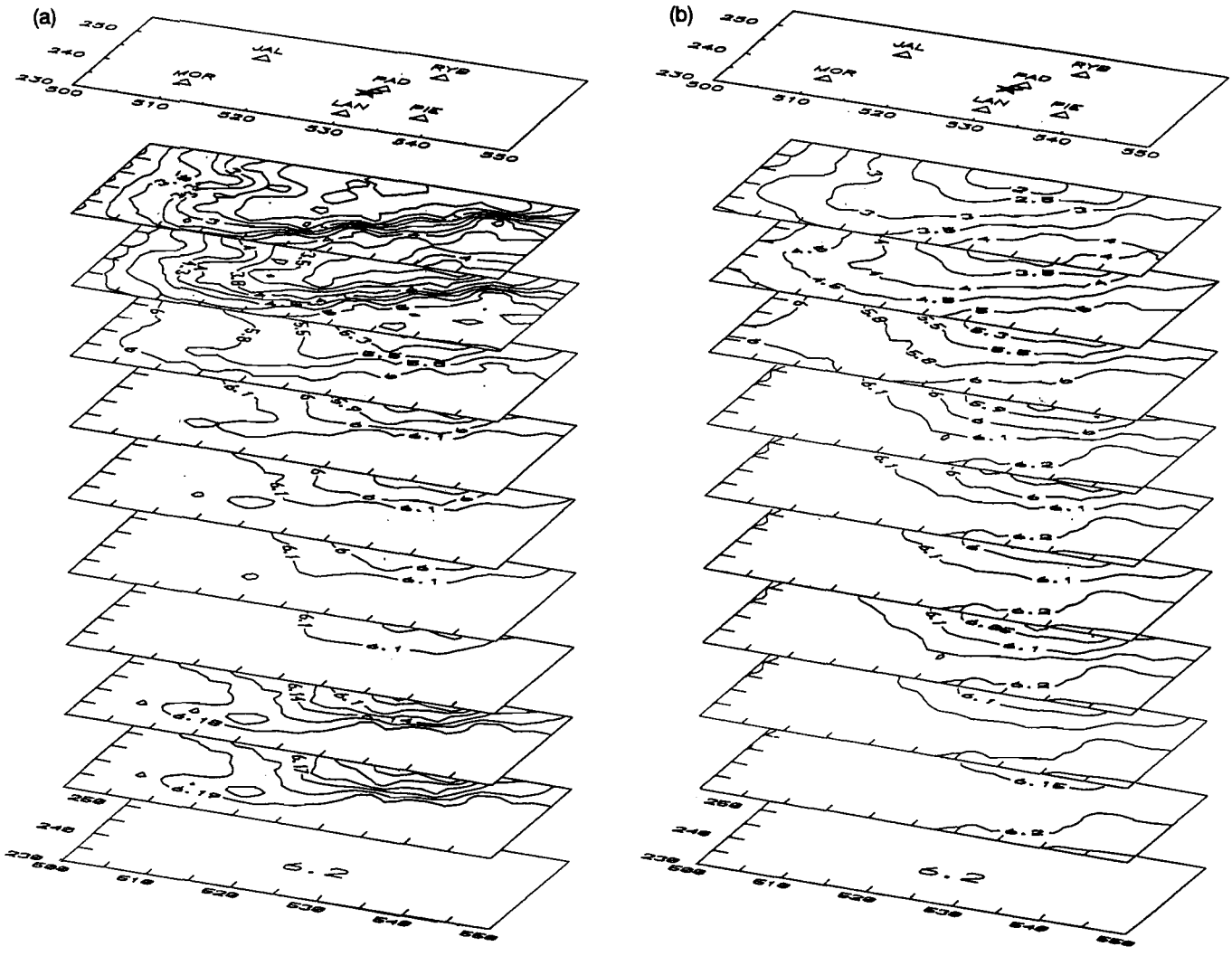

Figure 10. Structural models of the extended region of Dobrá Voda, Slovakia. (a) 3-D inhomogeneous model, (b) smoothed 3-D inhomogeneous model. Here v_P isolines are shown for the depth levels 0, 1.7, 3.3, 5, 6.7, 8.3, 10, 11.7, 13.3 and 15 km. Above the model the station distribution (triangles) and epicentre of the investigated event (asterisk) are depicted. Coordinates in kilometres.

bottom of Fig. 12), only the values of structural parameters for station JAL and, in part, station RYB differ substantially. In the case of JAL, the large error can be attributed to the small weight given to this station during the course of least-squares inversion due to its low amplitudes. The difference of final values of the structural parameter for RYB station may indicate an opposite effect of hypocentre adjustment and structural interpolation for this ray path.

In the course of inversions (3) and (4) the hypocentre was allowed to move inside a rectangular box $4 \times 4 \times 4$ km centred on the point found by kinematic localization (see Fig. 13). The hypocentre was shifted to a vertex of the box which indicates a small sensitivity of the solution to changes of the hypocentral coordinates in the example treated (note that kinematic information was excluded during this inversion).

The mechanisms are very similar in all four cases investigated. Decomposition of the moment tensor yields both a volumetric component (24 per cent) and a deviatoric component which comprises both DC (31 per cent) and CLVD (45 per cent) (see Fig. 14). However, an error ellipse constructed for the vector **L** on the basis of estimated variance of noise in the data reveals that at the 95 per cent confidence level a nearly deviatoric source is acceptable as well. The DC part of the mechanism is a nearly vertical dip-slip striking north, which is in agreement with the tectonics of this area according to which a fault with a N–S orientation exists in the region. The source time function retrieved exhibits a well-pronounced peak with width of about 20 ms, the rest being zero with respect to the uncertainty of the solution imposed by noise in the data.

CONCLUSIONS

The described method of determination of the mechanism and source time function of a point source by waveform inversion was tested on synthetic data generated for a configuration of a local seismic network consisting of five three-component stations, situated in the Dobrá Voda region, Slovakia. Tests using both *P* and *S* phases and only *P*

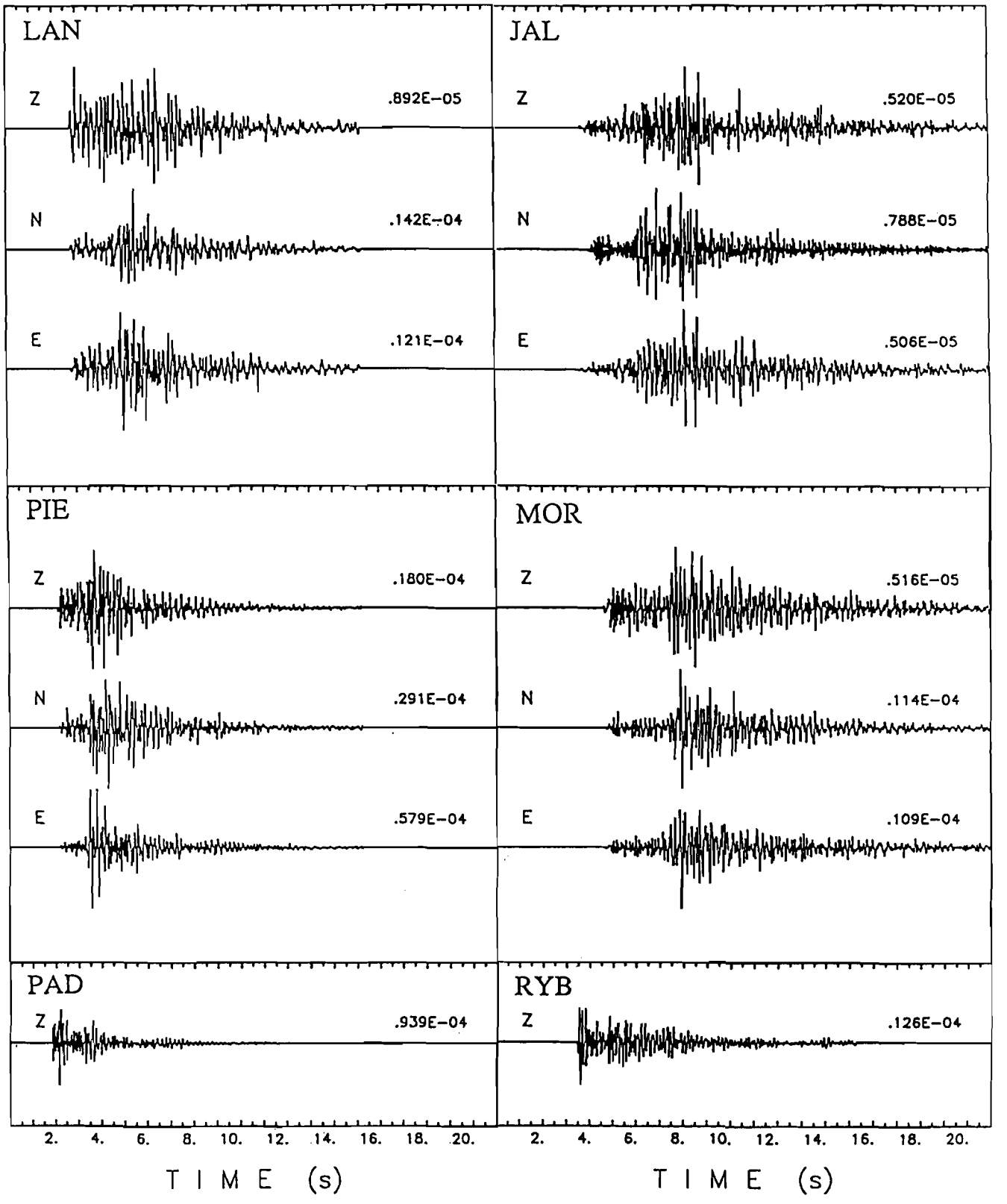

Figure 11. Velocity records of a local earthquake (local magnitude about 2) which occurred in the region of Dobrá Voda, Slovakia. The event was recorded by four three-component stations (LAN, PIE, JAL, MOR) and two vertical component stations (PAD, RYB).

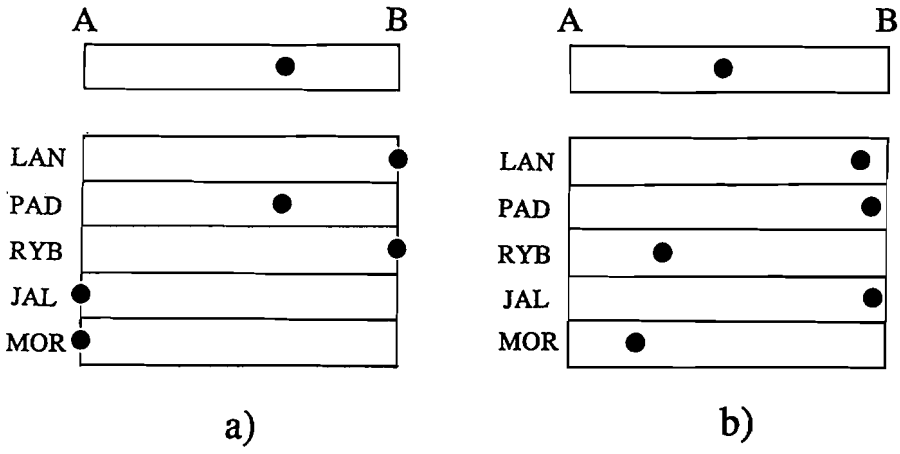

Figure 12. Results of structural optimization performed with one common structural weighting parameter for all the stations (upper part) and separately for each source-to-station path (lower part). (a) Inversion with hypocentre fixed at the point of kinematic localization, (b) inversion with hypocentre allowed to move inside a $4 \times 4 \times 4$ km box situated around the point specified by kinematic localization. Circles—resolved values of structural parameters.

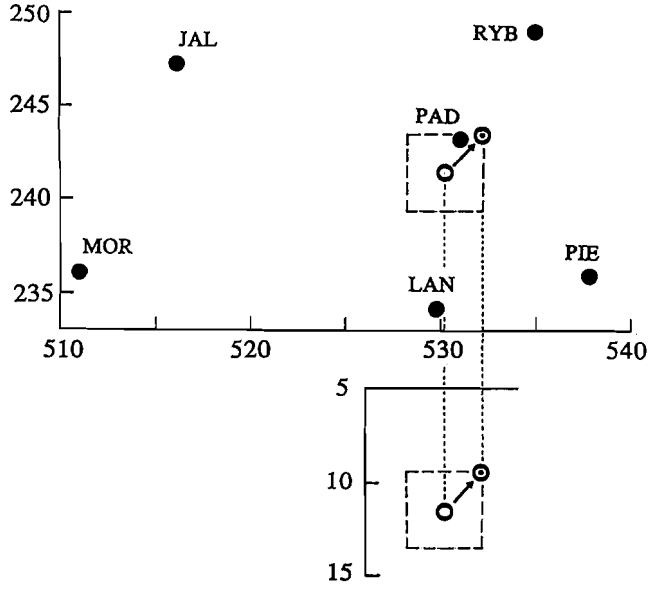

Figure 13. Dynamic relocalization of the earthquake in the Dobrá Voda region during the waveform inversion. Open circle—kinematic hypocentre (upper part, plane view; lower part, front view); open circle with dot—the hypocentre after relocalization; full circles—stations. Both horizontal coordinates and depth in kilometres.

phases yielded good resolution of a strike-slip mechanism, the resolution of a dip-slip mechanism being slightly worse but still acceptable. In all the experiments with synthetic noise-free data the source time function was determined very well.

As a by-product, the method allows us to optimize the hypocentre localization by interpolation of Green's functions constructed in a grid around the hypocentral point determined by kinematic localization. It can be advantageous in cases where the onsets of the seismic waves used for kinematic localization are not sharp enough, because the waveform modelling satisfies preferably large amplitudes in the records. In the tests performed the horizontal coordinates were optimized properly; failure of optimization of the hypocentral depth was probably caused by the small sensitivity of Green's functions to changes of the z-component of the hypocentre.

An additional option allows us to optimize, in a simplistic way, the model of the medium: interpolation of the Green's functions constructed for two slightly different structural models is performed which provides us with information as to which of the models is more convenient. This can be done for all the network at once or for each station separately. Synthetic tests revealed the success of this structural interpolation if performed for all the network; in the latter case the success depends on the sensitivity of individual ray paths to changes to the model.

The error analysis implemented in the inversion method transforms the variance of a noise present in the observed seismograms into confidence ellipses for the volumetric part, double-couple and compensated linear vector dipole components and for the T, N and P axes of the moment tensor retrieved. This allows us at an *a priori* selected confidence level to estimate the error in decomposition of the moment tensor into volumetric, DC and CLVD components and errors in determining the orientation of its deviatoric component.

Synthetic tests demonstrate that contamination of input data by a strong noise results in a large volumetric component of the mechanism. This can be explained by the fact that the random noise has no directivity and thus, if attributed to the source, contributes to its isotropic (i.e. the volumetric) component. However, the confidence region constructed for the solution of moment tensor decomposition reveals a low credibility of the volumetric component in such a case. In addition, the synthetic tests suggest that the presence of noise in the records being inverted affects the source time function determination more than the source mechanism retrieval.

For the inversion of the real event—a weak earthquake in the Dobrá Voda region, Slovakia—the data set was limited to very short sections of direct P waves, because no adequate model of the medium was available for modelling the later phases. The inversion resulted in a single pulse source time function and a mechanism containing all the

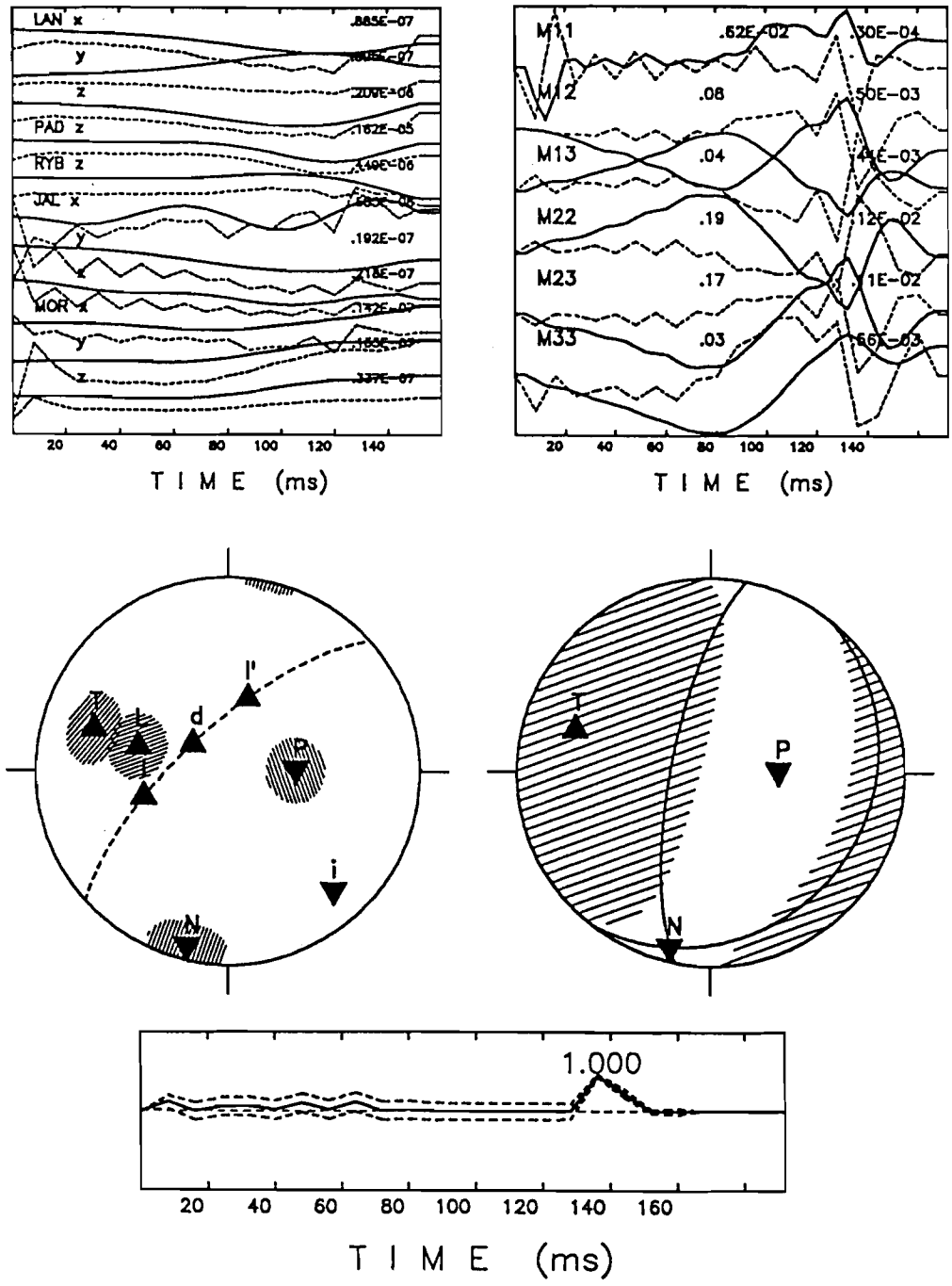

Figure 14. Inversion of seismograms of a local event in the Dobrá Voda region. For details see the caption of Fig. 9.

components; however, with respect to noise present in the records, at the 95% confidence level a nearly deviatoric source is acceptable as well. The DC component corresponds to a dip-slip striking north, which is in agreement with local tectonics.

ACKNOWLEDGMENTS

The records of the real event processed and the velocity models of the Dobrá Voda region were provided by Dr J. Sekeréš from Energoprojekt, Trnava. The authors appreciate the help of Dr V. Vavryčuk, the Geophysical Institute, the Czech Academy of Sciences, Prague, with polarization analysis of the records from this region. Comments and suggestions of an anonymous reviewer helped greatly to improve the text. The work was partly supported by an internal grant of the Czech Academy of Sciences. Part of the work was done during the fellowship of J.Š. at the International Centre for Theoretical Physics, Trieste, Italy.

REFERENCES

Aki, K. & Richards, P.G., 1980. *Quantitative Seismology*, Freeman, San Francisco.

Anderson, J.G., 1991. Strong motion seismology, *Rev. Geophys. Suppl.*, **29**, 700–720.

Červený, V., Molotkov, I. & Pšenčík, I., 1977. *Ray Method in Seismology*, Charles University Press, Praha.

Feignier, B. & Young, R.P., 1992. Moment tensor inversion of induced microseismic events: evidence of non-shear failures in the $-4 < M < -2$ moment magnitude range, *Geophys. Res. Lett.*, **19**, 1503–1506.

Kanamori, H., Ekström, G., Dziewonski, A., Barker, J.S. & Sipkin, S.A., 1993. Seismic radiation by magma injection: an anomalous seismic event near Tori Shima, Japan, *J. geophys. Res.*, **98**, 6511–6522.

Koch, K., 1991a. Moment tensor inversion of local earthquake data—I. Investigation of the method and its numerical stability with model calculations, *Geophys. J. Int.*, **106**, 305–319.

Koch, K., 1991b. Moment tensor inversion of local earthquake data—II. Application to aftershocks of the May 1980 Mammoth Lakes earthquakes, *Geophys. J. Int.*, **106**, 321–332.

Langston, C.A., 1981. Source inversion of seismic waveforms: the Koyna, India earthquakes of 13 September 1967, *Bull. seism. Soc. Am.*, **71**, 1–24.

Nábělek, J.L., 1984. Determination of earthquake source parameters from inversion of body waves, *PhD thesis*, MIT.

Oldenburg, D.W., 1982. Multichannel appraisal deconvolution, *Geophys. J. R. astr. Soc.*, **69**, 405–414.

Riedesel, M.A. & Jordan, T.H., 1989. Display and assessment of seismic moment tensors, *Bull. seism. Soc. Am.*, **79**, 85–100.

Ruff, L.J. & Tichelaar, B.W., 1990. Moment tensor rate functions for the 1989 Loma Prieta earthquake, *Geophys. Res. Lett.*, **17**, 1187–1190.

Šílený, J. & Panza, G.F., 1991. Inversion of seismograms to determine simultaneously the moment tensor components and source time function for a point source buried in a horizontally layered medium, *Stud. geophys. geod.*, **35**, 166–183.

Šílený, J., Panza, G.F. & Campus, P., 1992. Waveform inversion for point source moment tensor retrieval with variable hypocentral depth and structural model, *Geophys. J. Int.*, **109**, 259–274.

Sipkin, S.A., 1982. Estimation of earthquake source parameters by the inversion of waveform data: synthetic waveforms, *Phys. Earth planet. Inter.*, **30**, 242–259.

Stickney, M.C. & Sprenke, K.F., 1993. Seismic events with implosional focal mechanisms in the Coeur d'Alene mining district, Northern Idaho, *J. geophys. Res.*, **98**, 6523–6528.

Tarantola, A., 1987. *Inverse Problem Theory. Methods for Data Fitting and Model Parameter Estimation*, Elsevier, Amsterdam.

Vasco, D.W., 1989. Deriving source-time functions using principal component analysis, *Bull. seism. Soc. Am.*, **79**, 711–730.

Wong, I.G. & McGarr, A., 1990. Implosional failure in mining-induced seismicity: a critical review, in *Proc. 2nd International Congress on Rockbursts and Seismicity in Mines*, Minneapolis, pp. 45–51, Balkema, Rotterdam.

Wong, I.G., Humprey, J.R., Adams, J.R. & Silva, W.J., 1989. Observation of mine seismicity in the eastern Wasatch Plateau, Utah, U.S.A.: possible case of implosional failure, *Pure appl. Geophys.*, **129**, 369–405.

APPENDIX: MINIMIZATION OF $N_s(q_l)$

Linearization

In a $\Delta\mathbf{q}$ vicinity of a point $\mathbf{q}^0$ we expand the Green's function in the Taylor series and keep the first two terms only:

$$\phi_{il}^k(t, \mathbf{q}) \cong \phi_{il}^k(t, \mathbf{q}^0) + \sum_{j=1}^{M} \left.\frac{\partial \phi_{il}^k}{\partial q_j}\right|_{\mathbf{q}=\mathbf{q}^0} \Delta q_j, \tag{A1}$$

where Φ_{il}^k is the Green's function after renotation for the ith displacement component in the kth station, where the index l was used to substitute the indices m,n:

$$g_{im,n}^k \Rightarrow \Phi_{il}^k \qquad \begin{aligned} &k = 1, \ldots, N, \\ &i, m, n = 1, \ldots, 3, \\ &l = 1, \ldots, 6. \end{aligned}$$

Here $M = 4$ or $M = N + 3$ is the number of q_l parameters. Then, inserting eq. (A1) into eq. (2) yields the ith component of the displacement at the kth station:

$$u_i^k(t) \cong u_i^k(t)|_{\mathbf{q}^0} + \sum_{j=1}^{M} v_{ij}^k(t)|_{\mathbf{q}^0} \Delta q_j, \tag{A2}$$

where

$$u_i^k(t)|_{\mathbf{q}^0} = \sum_{l=1}^{6} F_l(t) \otimes \phi_{il}^k(t, \mathbf{q}^0),$$

$$v_{ij}^k(t)|_{\mathbf{q}^0} = \sum_{l=1}^{6} F_l(t) \otimes \left.\frac{\partial \phi_{il}^k}{\partial q_j}\right|_{\mathbf{q}=\mathbf{q}^0}.$$

Here $F_l(t)$, $l = 1, \ldots, 6$, are functions $\dot{M}_{ij}(t)$, $i = 1, \ldots, 3$, $j = i, \ldots, 3$, after renotation.

The condition of a minimum of $N_s(q_l)$ requires zero partial derivatives of the $N_s(q_l)$ with respect to q_l. This results in the system of linear equations

$$\mathbf{A}\Delta\mathbf{q} = \mathbf{b}, \tag{A3}$$

where $\mathbf{A}$ is a symmetric $M \times M$ matrix with elements

$$A_{pj} = \sum_{k=1}^{N} \sum_{i=1}^{3} \int_t v_{ip}^k(t)|_{\mathbf{q}^0} v_{ij}^k(t)|_{\mathbf{q}^0} \, dt,$$

$$b_p = \sum_{k=1}^{N} \sum_{i=1}^{3} \int_t [u_i^k(t)|^{\text{obs}} - u_i^k(t)|_{\mathbf{q}^0}] v_{ip}^k(t)|_{\mathbf{q}^0}(t) \, dt.$$

In the case of option (a) of the classification of the $\mathbf{q}$ parameters (see 'Theory') the $\mathbf{A}$ matrix is full; however, in the case of (b) it is sparse in the following way. Note that, for structural optimization separately for each of the stations, the Green's function Φ_{il}^k depends on q_j only if $j = k + 3$ (i.e. it depends on the q_{ij} parameter corresponding to this station only), which results in the $\mathbf{A}$ matrix in the form

$$\mathbf{A} = \begin{bmatrix} A_{11} & A_{12} & A_{13} & 0 & 0 & \cdots & 0 \\ A_{12} & A_{22} & A_{23} & 0 & 0 & \cdots & 0 \\ A_{13} & A_{23} & A_{33} & 0 & 0 & \cdots & 0 \\ 0 & 0 & 0 & A_{44} & 0 & \cdots & 0 \\ & & & & & & \\ 0 & 0 & 0 & 0 & 0 & \cdots & A_{MM} \end{bmatrix}.$$

The applicability of the linearization approach is limited by the validity of the expansion (A1). It can be used when second and higher derivatives of Φ_{il}^k are small. Problems are caused especially by the general dependence of arrival times of the Green's functions on the $\mathbf{q}$ parameters. The derivatives in eq. (A1) are estimated by differences and they can be accurate enough only if the time shift of arrival times

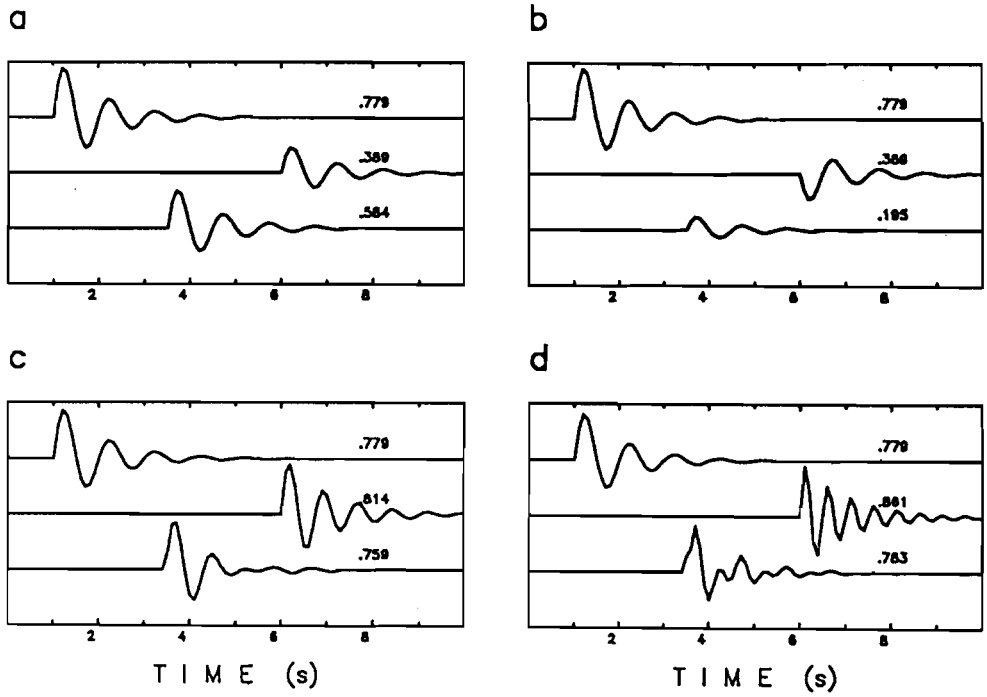

Figure A1. Example of interpolation of hypothetical time-delayed Green's functions (damped sine pulse). Upper and middle trace—the function in grid points 1 and 2, respectively; lower trace—interpolated function at the point $\xi = \frac{1}{2}$. (a and b) Function at grid points 1 and 2 of the same period $T = 1$ s and amplitude ratio equal to 2 (in b the sign of the function in grid point 2 is reversed). (c and d) Functions at grid points 1 and 2 of the same amplitudes and ratio of periods T_2/T_1 equal to 0.75 and 0.5, respectively.

in the interval used for the difference calculation is small with respect to the prevailing period of the Green's function T_g, $dt \ll T_g$. In conclusion, linearization may be used only for low-pass filtered data, for which the prevailing period of the Green's functions T_g is large enough in comparison with changes of the arrival time in the definition range of the **q** parameters. Since the above requirement can, in certain situations, be in conflict with conditions of applicability of the ray method, we propose and use an alternative approach described below.

Grid search for the minimum of $N_s(\mathbf{q})$

Because we want to invert local seismograms, which are, in general, high-frequency spiky records, it is more suitable to avoid linearization (see above) and to look for the minimum of $N_s(\mathbf{q})$ by evaluating directly the $N_s(\mathbf{q})$ in the space limited by definition ranges of the **q** parameters. With this approach we need to evaluate the Green's functions for floating points **q** on the basis of their exactly calculated values in *a priori* selected grid points. To do so the following interpolation scheme is used: let $F_1(t)$ and $F_2(t)$ be Green's functions in two neighbouring grid points 1 and 2, respectively, and let $F_2(t)$ be delayed by Δt with respect to $F_1(t)$. Then the Green's function at a point ξ between 1 and 2 within a distance ξ from point 1 is calculated according to the formula

$$F_\xi(t) = (1-\zeta)F_1(t - \zeta\Delta t) + \zeta F_2[t + (1-\zeta)\Delta t], \qquad \text{(A4)}$$

where $\zeta = \xi/D$, and D is the distance between points 1 and 2. This scheme linearly interpolates both the arrival time and amplitudes of the function at a point ξ. It is demonstrated in Fig. A1, which shows an example of interpolation of a damped sine function. The upper and middle traces in each frame depict the function at points 1 and 2, the lower trace shows the interpolated function at the point $\xi = D/2$. In Fig. A1(a) both F_1 and F_2 are of the same frequency, the F_2 function having amplitudes half of those of the function F_1. In Fig. A1(b) there is the same situation, only the sign of F_2 is reversed. In both cases because of constant frequency the shape of F_1 is reproduced in F_ξ. In Figs A1(c) and (d) an example is presented where the frequency of F_2 differs from that of F_1 (this example simulates a more general case when the Green's function may change its shape also). The ratio of frequencies of F_1 and F_2 is 0.75 and 0.5 in Figs A1(c) and (d) respectively. While in Fig. A1(c) the resultant F_ξ is reasonable (it roughly retains the shape of a damped sine function with a period between the periods of F_1 and F_2), in Fig. A1(d) its shape is damaged due to too different frequencies of F_1 and F_2, which suggests that in the hypothetical case (d), the grid for computing the Green's functions should have been made more dense.

The situation is much simpler in the cases considered throughout this paper, because in elastic media the Green's functions are narrow pulses and no problems are encountered during interpolation.